



Article

Photoelectrochemical Performance Observed in Mn-Doped BiFeO₃ Heterostructured Thin Films

Hao-Min Xu ¹, Huanchun Wang ^{1,2}, Ji Shi ³, Yuanhua Lin ^{1,*} and Cewen Nan ¹

¹ State Key Laboratory of New Ceramics and Fine Processing, School of Materials Science and Engineering, Tsinghua University, Beijing 100084, China; xuhm13@mails.tsinghua.edu.cn (H.-M.X.); wanghc12@mails.tsinghua.edu.cn (H.W.); cwnan@mail.tsinghua.edu.cn (C.N.)

² High-Tech Institute of Xi'an, Xi'an 780025, China

³ Department of Metallurgy and Ceramics Science, Tokyo Institute of Technology, 2-12-1, Ookayama, Meguro-ku, Tokyo 152-8552, Japan; shi.j.aa@m.titech.ac.jp

* Correspondence: linyh@mail.tsinghua.edu.cn; Tel.: +86-10-6277-3741

Academic Editor: Hongqi Sun

Received: 9 October 2016; Accepted: 11 November 2016; Published: 16 November 2016

Abstract: Pure BiFeO₃ and heterostructured BiFeO₃/BiFe_{0.95}Mn_{0.05}O₃ (5% Mn-doped BiFeO₃) thin films have been prepared by a chemical deposition method. The band structures and photosensitive properties of these films have been investigated elaborately. Pure BiFeO₃ films showed stable and strong response to photo illumination (open circuit potential kept -0.18 V, short circuit photocurrent density was -0.023 mA·cm⁻²). By Mn doping, the energy band positions shifted, resulting in a smaller band gap of BiFe_{0.95}Mn_{0.05}O₃ layer and an internal field being built in the BiFeO₃/BiFe_{0.95}Mn_{0.05}O₃ interface. BiFeO₃/BiFe_{0.95}Mn_{0.05}O₃ and BiFe_{0.95}Mn_{0.05}O₃ thin films demonstrated poor photo activity compared with pure BiFeO₃ films, which can be explained by the fact that Mn doping brought in a large amount of defects in the BiFe_{0.95}Mn_{0.05}O₃ layers, causing higher carrier combination and correspondingly suppressing the photo response, and this negative influence was more considerable than the positive effects provided by the band modulation.

Keywords: photocatalysis; photoelectrochemical; solar energy conversion; Mn-doped BiFeO₃ films; heterostructure

1. Introduction

BiFeO₃ (BFO) is famous for its room temperature multiferroic properties, but it is attracting more and more interest as a small band gap photo-ferroelectric material. In the past few years, photocatalytic (PC), and photovoltaic (PV) properties of BFO films have been studied [1–5]. For example, polycrystalline BFO photo electrode was applied for water photo-oxidation [6]; an enhanced ferroelectric PV response of multilayered BiFeO₃/BaTiO₃ was observed [7]. The photoelectrochemical (PEC) response of BFO with ferroelectric materials has also been reported [8,9]. Findings imply the promising potential applications of BFO films in terms of photocatalysts, photovoltaic cells, multifunction sensors, etc. [10–12].

High quality photocatalysts, or the PEC electrodes, are believed to possess high-energy conversion efficiency. One of the key issues for energy conversion performance is the ability of light absorption, which is mostly decided by the band gap of the material. Element doping is quite a normal method in band engineering. Usually, metal element doping does better in narrowing the band gap than the anions do [13]. More specifically, to narrow the band gap of BFO, people can conduct A/B-site doping with elements such as La [14], Gd [15], Y and Ti [16]. The A-site and B-site represents the positions of Bi and Fe atoms in the BFO lattice, respectively. B-site Mn doping is a potential method of modifying the band structure of BFO [17]. The Mn element has attracted great attention due to its special role in BFO thin films. For example, people found that BFO films showed enhanced ferroelectric and

weak magnetic behaviors by 5% Mn substitution [18,19]. Optical and PC properties of Mn-involved co-doping BFO have also been recently studied. For example, researchers observed that Ba/Ca and Mn co-doped BFO nanofibers delivered enhanced PC performances [20,21]; Vinay et al. obtained a photo-induced current of about 250-fold in Ce and Mn co-doped BFO thin films at zero bias in a PV test [5]. However, few studies have focused on the effects of the Mn single doping of BFO on PEC properties. In this work, we set Mn doping content as 0.05, preparing $\text{BiFe}_{0.95}\text{Mn}_{0.05}\text{O}_3$ thin films, and studied their optical and PEC properties.

Furthermore, the energy conversion is highly restricted by the combination of photo-induced electro-hole pairs, which can happen inside or on the surface of the material. How to separate these pairs much more efficiently has been a question for a long time [22]. According to the research before, we know that the internal field plays an important role in separating e-h pairs; through studying the principles of the internal field, we are able to create or design an internal field that could provide more effective electron-hole separation, faster interface charge transfer, and longer carrier lifetime. For example, using the polarization in the ferroelectric materials [9,23,24], constructing the p-n junction or polymorph junction can work appropriately [25]. Considering these facts, it would be interesting to construct a heterostructure with BFO and band-modified BFO, and study the effects of internal field built around boundary on PEC activity. Therefore, in the present work, we made heterostructured BFO/ $\text{BiFe}_{0.95}\text{Mn}_{0.05}\text{O}_3$ (BFMO) films and investigated their PEC properties.

2. Results and Discussion

X-ray diffraction (XRD) results are shown in Figure 1. All peaks in the XRD patterns of the BFO films are indexed for a rhombohedral structure with R3m symmetry and were found to be in good agreement with the corresponding values reported in the PDF#14-0181, while the BFMO films display a structure transition according to the (012) and (110) peaks that were changed, and the (021) peak with the three peaks around $2\theta = 56^\circ\text{--}57.1^\circ$ disappeared. The peaks of the BFMO films fit well with the tetragonal BiMnO_3 reported in PDF#53-0767, which implies that the film structure has partly transferred from rhombohedral to tetragonal due to the Mn doping. Similar results have been reported previously [18]. From the XRD patterns, we can also see that BFMO did not crystallize as well as BFO. Both the BFO film and the BFMO film is densely crystallized according to the scanning electron microscopy (SEM) images of the surface morphology of the films (Figure 2a,b).

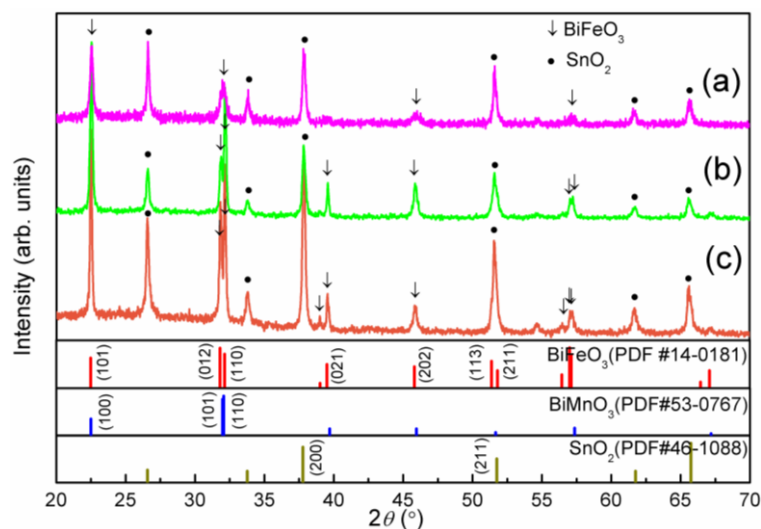


Figure 1. X-ray diffraction (XRD) patterns of (a) $\text{BiFe}_{0.95}\text{Mn}_{0.05}\text{O}_3$ (BFMO); (b) BiFeO_3 (BFO)/BFMO and (c) BFO films. PDF#14-0181 shows BFO in rhombohedral structure, and PDF#53-0767 shows BFMO in tetragonal structure, PDF#46-1088 shows the peak positions of SnO_2 substrate.

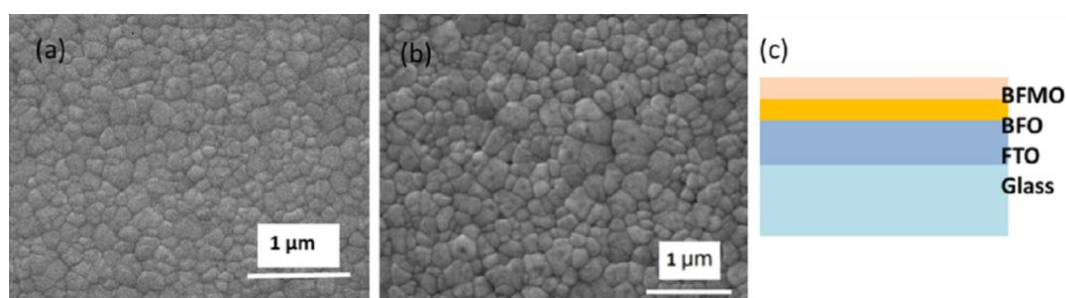


Figure 2. The surface scanning electron microscopy images of (a) BFO and (b) BFMO film; (c) The illustration of BFO/BFMO heterostructure.

To test the photo-response ability of our films, we first tested the PEC properties of BFO. According to the $I-t$ measurements (Figure 3, 0 V bias) and $P-t$ (Figure 4a, BFO), we observed a repeatable and stable instantaneous response to the light illumination, coming along with a photocurrent density $-0.023 \text{ mA}\cdot\text{cm}^{-2}$ and an open circuit potential (OCP) -0.18 V when exposed to light, proving again the high sensitivity of BFO films to light. The $-0.023 \text{ mA}\cdot\text{cm}^{-2}$ photocurrent density at zero bias voltage was much larger than previous reports [8,26]. The $I-t$ test with the varied initial potentials of BFO (Figure 3) implies that a negative initial potential can improve the photo response, while a positive one will weaken the response, which can be explained by the fact that negative OCP appears under photo illumination, and the photo-induced electrons aggregating on the F-doped SnO_2 (FTO) side have to get over the barrier that the positive applied voltage creates to move out to the counter electrode. The dark current density increased to $-0.005 \text{ mA}\cdot\text{cm}^{-2}$ at an applied potential of -0.4 V , which is much smaller than previous reports [26].

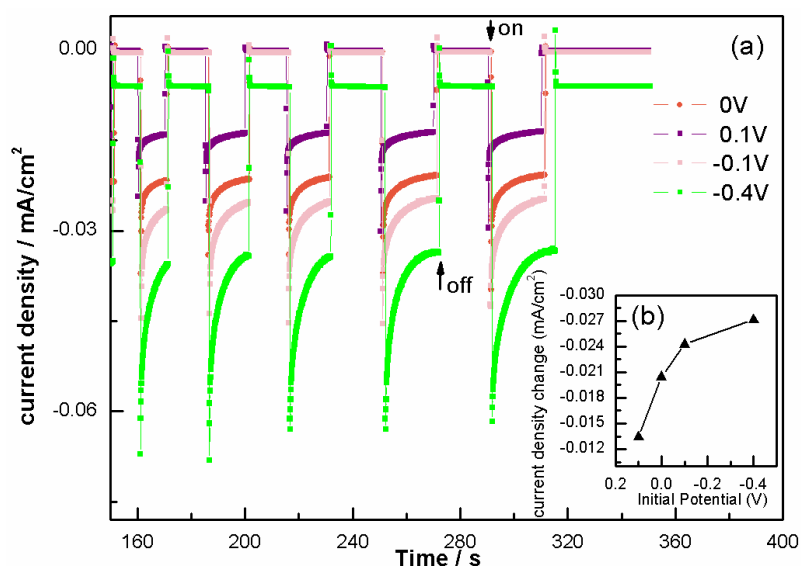


Figure 3. (a) $I-t$ curves of BFO at 0 V, 0.1 V, -0.1 V and -0.4 V bias voltages; inset (b) is the photocurrent density change under different bias voltages.

Then, we tested the photo-response ability of BFMO films and the heterostructured BFO/BFMO films and compared them with BFO films. BFMO displayed a nearly 0 V OCP, and BFO/BFMO appeared to be unstable, with only a quarter OCP to BFO (Figure 4a). In Figure 4a, the initial position of the three types varied because of the different surface state contrast to the reference electrode. The time dependence of the photocurrent density measurements at 0 V, 0.1 V and -0.4 V bias voltages are shown in Figure 4b–d. BFMO films and the BFO/BFMO films barely had an obvious photocurrent.

The values are still small, even when applying a negative voltage. Even though Mn doping in BFO will always induce a low leakage current (the dark current intensity of BFMO at 0 V is $8 \times 10^{-4} \text{ mA}\cdot\text{cm}^{-2}$, slightly larger than BFO of $2.5 \times 10^{-4} \text{ mA}\cdot\text{cm}^{-2}$), it cannot affect the photocurrent that much, since the dark current intensity of BFO/BFMO is $9 \times 10^{-5} \text{ mA}\cdot\text{cm}^{-2}$, much smaller than BFO. According to the $I-t$ results of BFMO and BFO/BFMO films, the transient anode photocurrent upon light illumination was small and attenuated quickly, indicating the strong recombination and short life of photo-induced carriers. In general, pure BFO film performs best compared with BFMO and the heterostructured BFO/BFMO films.

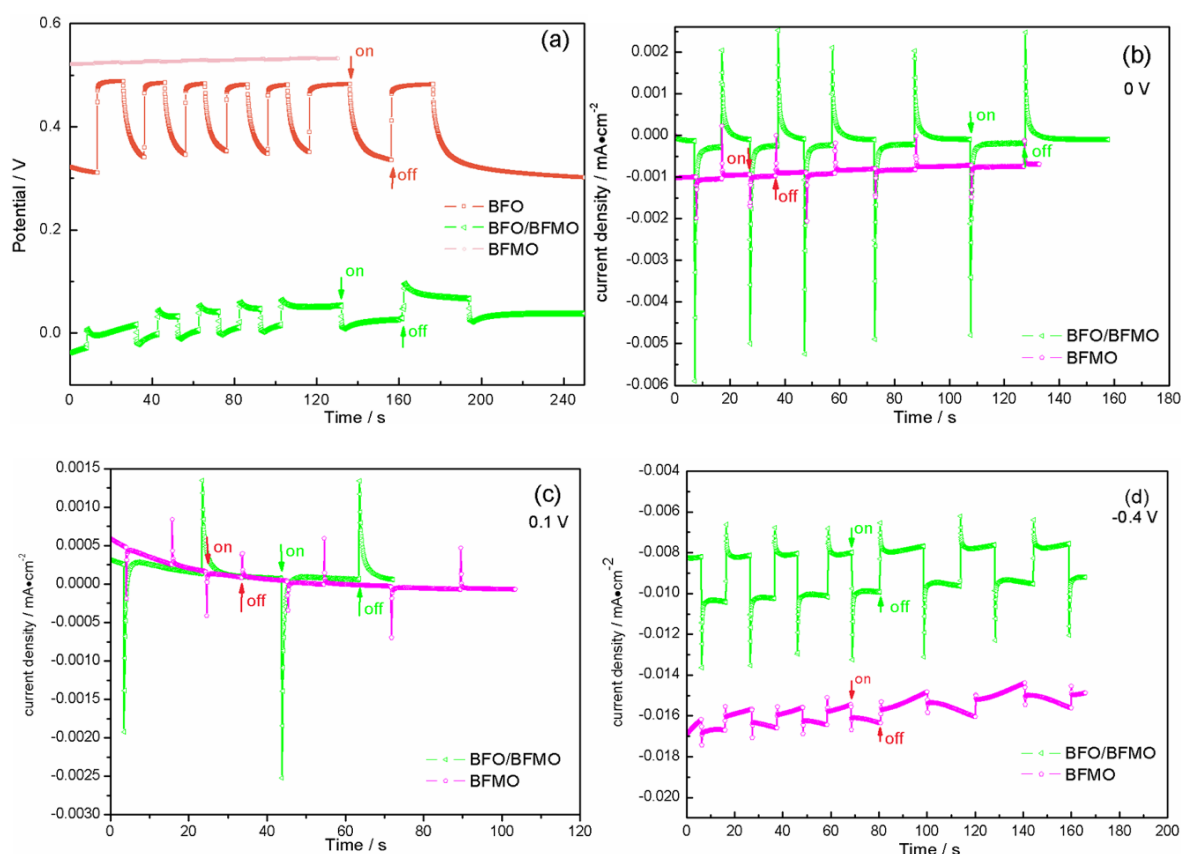


Figure 4. (a) Open circuit potential tests of the three types of samples under on-off $150 \text{ mW}/\text{cm}^2$ light illumination. $I-t$ curves at (b) 0 V; (c) 0.1 V; (d) -0.4 V of BFMO and BFO/BFMO films.

To explain the phenomenon above, the energy band structures of the films were carefully investigated. Ultraviolet-visible (UV-Vis) absorption measurements and the band gap calculations (shown in Figure 5) indicate that BFMO cannot absorb light as much as BFO does, and it has a band gap of 2.39 eV, which is smaller than BFO's band gap of 2.60 eV. To get an insight into how the band structure of BFO changes via Mn doping, and to understand the internal field built around the boundary of heterostructured BFO/BFMO, several methods were applied to determine the band position of BFO and BFMO in the heterostructured BFO/BFMO. The first method relies on the following formula:

$$E_C = X - E_v - \frac{1}{2}E_g \quad (1)$$

where E_C presents the position of conductive band (CB), X is the absolute electronegativity of the semiconductor, E_e is the energy of free electrons on the hydrogen scale, and E_g is the band gap of the semiconductor. The theoretical band positions are shown in Figure 6c. The second method is represented by using X-ray photoelectron spectroscopy (XPS) valance spectra in Figure 6a, which can explain E_v , the position of valence band (VB) in Figure 6d, but it is not accurate enough [27]. The third method is the Mott–Schottky method, which is conducted by the electrochemical station. The Mott–Schottky equation is as follows:

$$\frac{1}{C^2} = \frac{2}{\epsilon\epsilon_0 A^2 e N_D} \left(V - V_{fb} - \frac{k_B T}{e} \right) \quad (2)$$

where C is space charge layers capacitance, e is electron charge, ϵ is dielectric constant, ϵ_0 means permittivity of vacuum, N_D = electron donordensity, V means applied potential, k_B is Boltzmann's constant, T is absolute temperature, and V_{fb} is flat band potential [28]. In the function of $1/C^2$ and applied potential (V), $V_{fb} + \frac{k_B T}{e}$ can be determined by taking the x-intercept of a linear fit to the Mott–Schottky plot (shown in Figure 6b), and $\frac{k_B T}{e}$ was calculated as 0.0259 V. Thus, the V_{fb} of BFO is estimated as -0.33 V (vs. Ag/AgCl) or 0.27 V (vs. reversible hydrogen electrode, RHE), and BFMO is -0.41 V (vs. Ag/AgCl) or 0.20 V (vs. RHE). To convert the obtained potential (vs. Ag/AgCl) to RHE, the following equation [29] was used:

$$E(\text{RHE}) = E(\text{Ag/AgCl}) + 0.059 \text{ pH} + 0.21 \quad (3)$$

For n-type semiconductors, the flat-band potential (V_{fb}) was considered to be located just under the CB; hence, we can calculate the band position as shown in Figure 6e [6]. Even though the band positions obtained by the three methods were found to vary, one fact is that they can all be classified into the structure shown in Figure 6f, in which the band bends and benefits the separation of photogenerated e–h.

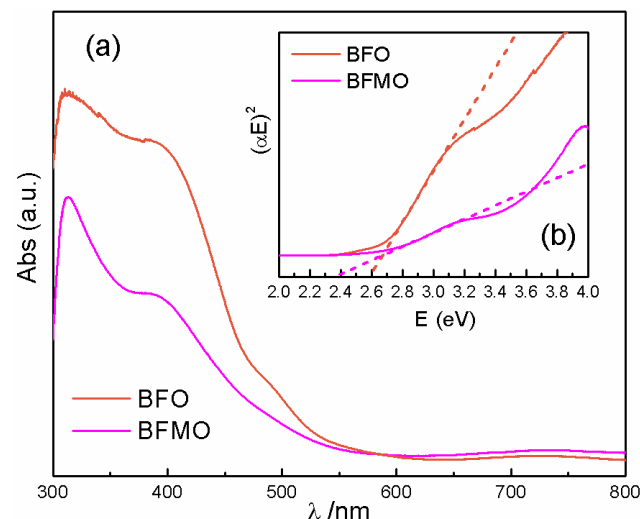


Figure 5. (a) Ultraviolet-visible (UV-Vis) absorption spectra of BFO and BFMO; (b) the band gap calculation.

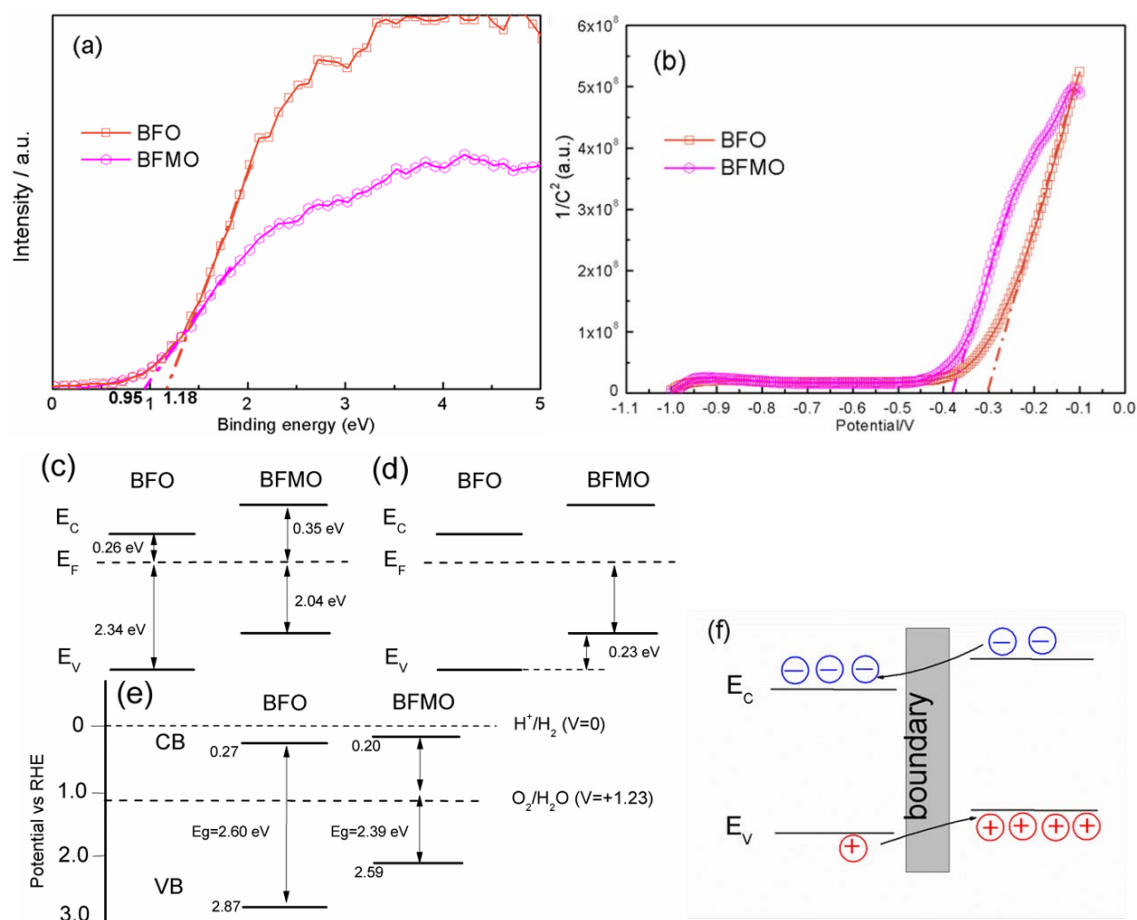


Figure 6. (a) X-ray photoelectron spectroscopy (XPS) valence spectra; (b) Mott–Schottky curve; the band position determined by (c) theoretical calculation, (d) XPS valence spectra method and (e) Mott–Schottky method; (f) an illustration of carriers transferring through boundary.

Although BFMO has a smaller band gap than BFO, and BFO/BFMO films own an advantageous band bend causing an internal field, pure BFO film performs best compared with BFMO and the heterostructured BFO/BFMO films. These facts imply that another factor influencing the photo response, which exceeds the effect of more light absorption, exists in the BFMO layers and the band bend in the interface of BFO/BFMO. On the basis of the XRD patterns (Figure 1), the inferior crystallinity of BFMO implied more vacancy defects in the BFMO films. More vacancy defects in BFMO can also be determined in photo-luminescence (PL) spectra (Figure 7). The fluorescence effect is a little bit higher in BFMO than in BFO films, which might be attributed to the higher e–h combination occurring around the defects. The doping process could generate more defects in BFMO, and the consequent higher e–h combination considerably decreased the PEC properties of BFMO and BFO/BFMO films. Nevertheless, Mn single doping does not cause detrimental effects on photo response of all material systems; for example, Mn single doping into the TiO_2 lattice results in a significant enhancement in photoabsorption and in the quantity of photogenerated hydroxyl radicals due to the formation of a low oxygen-vacancy content [30].

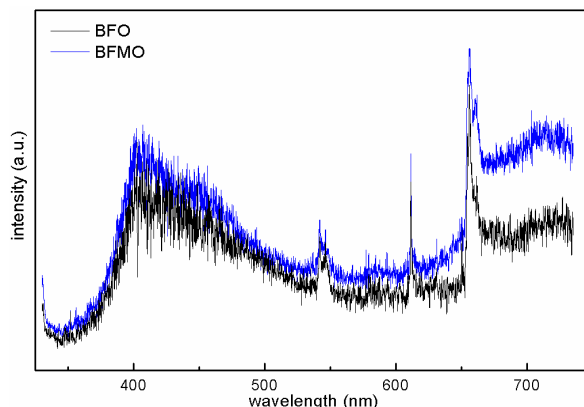


Figure 7. Photo-luminescence spectra of BFO and BFMO films.

3. Materials and Methods

The BFO films were fabricated on FTO substrates as reported previously [10]. To get the 5% Mn-doped BFO, we chose $C_4H_6MnO_4 \cdot 4H_2O$ as the Mn source. The BFO film is 4-layered, the BFMO film is 4-layered, and the heterostructured BFO/BFMO film (shown in Figure 2c) is combined by 2-layered BFO and 2-layered BFMO. One layer represents one instance of spin coating.

XRD was carried out to analyze the crystal structure by X-ray diffractometer (RIGAKU D/max 2500, Tokyo, Japan) with Cu radiation at 40 kV/200 mA. The XRD scanning speed was $6^\circ/\text{min}$ (standard configuration). The microstructures were checked by field emission microscope at 20 kV (JSM-7001F, JEOL, Tokyo, Japan). UV-Vis absorption spectra were measured by a UV-Vis spectrophotometer (UV-3310, HITACHI, Tokyo, Japan). The PL spectra were tested with LabRAM HR Evolution (HORIBA, Kyoto, Japan), and the incident laser wave length was 325 nm. XPS valance spectrum was tested by PHI Quantera SXM (ULVAC-PHI, INC., Tokyo, Japan).

The PEC measurements, including the time dependence open circuit potential ($P-t$), the time dependence of the photocurrent density ($I-t$) was carried out by an electrochemistr workstation (CHI 660D, CHENHUA, Shanghai, China) in a three-electrode cell. The prepared samples, a small Pt foil, and a saturated Ag/AgCl were used as the working electrode, the counter electrode, and the reference electrode, respectively. 0.1 M Na_2SO_4 (at pH = 6.7) was used as the electrolyte. The working electrode was illuminated under $150 \text{ mW}/\text{cm}^2$ visible-light irradiation ($\lambda > 420 \text{ nm}$). $I-t$ was measured in the light on-off process with a pulse of 10–50 s by the potentiostatic technique at 0 V, -0.1 V , 0.1 V and -0.4 V bias versus Ag/AgCl.

4. Conclusions

In this work, we carried out band engineering on BFO films via Mn doping and prepared heterostructured BFO/BFMO films. The photo-response activities of these films were studied through PEC tests. The pure BFO film is sensitive to visible light, which is potentially applicable in photo-related fields, such as optical sensitive sensors, PV cells, and photocatalysts. In our heterostructured BFO/BFMO samples, the facilitating effects provided by the smaller band gap of the BFMO layer and the internal field in the interface on PEC performance cannot compensate the negative effect caused by the severe e-h combination in the BFMO layer. The combination of photogenerated charge carriers occurred around the defects introduced by Mn doping. The major results indicated that, to enhance the photo-response ability and improve energy conversion when designing a BFO based photic device, integrated multi-factors need to be taken into account. In addition, more theoretical work with respect to the separation mechanism of photogenerated charge carriers is desirable in the future.

Acknowledgments: This work was supported by the NSF of China (51532003, 51221291, and 51328203).

Author Contributions: Haomin Xu and Yuanhua Lin conceived and designed the experiments; Haomin Xu performed the experiments; Haomin Xu and Huanchun Wang analyzed the data; Cewen Nan and Yuanhua Lin contributed reagents/materials/analysis tools; Haomin Xu and Ji Shi wrote the paper.

Conflicts of Interest: The authors declare no conflict of interest.

References

1. Dong, W.; Guo, Y.; Guo, B.; Liu, H.; Li, H.; Liu, H. Enhanced photovoltaic properties in polycrystalline BiFeO₃ thin films with rhombohedral perovskite structure deposited on fluorine doped tin oxide substrates. *Mater. Lett.* **2012**, *88*, 140–142. [[CrossRef](#)]
2. Chen, B.; Li, M.; Liu, Y.; Zuo, Z.; Zhuge, F.; Zhan, Q.F.; Li, R.W. Effect of top electrodes on photovoltaic properties of polycrystalline BiFeO₃ based thin film capacitors. *Nanotechnology* **2011**, *22*, 195201. [[CrossRef](#)] [[PubMed](#)]
3. Peng, Z.; Liu, B. Photoinduced changes in the hysteresis loop and photovoltaic effect of the magnetron sputtered epitaxial BiFeO₃ film. *Phys. Status Solidi A* **2014**, *2*, 1–4.
4. Katiyar, R.K.; Sharma, Y.; Misra, P.; Puli, V.S.; Sahoo, S.; Kumar, A.; Scott, J.F.; Morell, G.; Weiner, B.R.; Katiyar, R.S. Studies of the switchable photovoltaic effect in co-substituted BiFeO₃ thin films. *Appl. Phys. Lett.* **2014**, *105*, 172904. [[CrossRef](#)]
5. Gupta, S.; Tomar, M.; Gupta, V. Ferroelectric photovoltaic properties of Ce and Mn codoped BiFeO₃ thin film. *J. Appl. Phys.* **2014**, *115*, 014102. [[CrossRef](#)]
6. Moniz, S.J.A.; Quesada-Cabrera, R.; Blackman, C.S.; Tang, J.; Southern, P.; Weaver, P.M.; Carmalt, C.J. A simple, low-cost CVD route to thin films of BiFeO₃ for efficient water photo-oxidation. *J. Mater. Chem. A* **2014**, *2*, 2922. [[CrossRef](#)]
7. Sharma, S.; Tomar, M.; Kumar, A.; Puri, N.K.; Gupta, V. Enhanced ferroelectric photovoltaic response of BiFeO₃/BaTiO₃ multilayered structure. *J. Appl. Phys.* **2015**, *118*, 074103. [[CrossRef](#)]
8. Cao, D.; Wang, Z.; Nasori, N.; Wen, L.; Mi, Y.; Lei, Y. Switchable charge-transfer in the photoelectrochemical energy-conversion process of ferroelectric BiFeO₃ photoelectrodes. *Angew. Chem. Int. Ed.* **2014**, *126*, 11207–11211. [[CrossRef](#)]
9. Wang, Z.; Cao, D.; Wen, L.; Xu, R.; Obergfell, M.; Mi, Y.; Zhan, Z.; Nasori, N.; Demsar, J.; Lei, Y. Manipulation of charge transfer and transport in plasmonic-ferroelectric hybrids for photoelectrochemical applications. *Nat. Commun.* **2016**, *7*, 10348. [[CrossRef](#)] [[PubMed](#)]
10. Xu, H.M.; Wang, H.C.; Shen, Y.; Lin, Y.-H.; Nan, C.W. Photocatalytic and magnetic behaviors of BiFeO₃ thin films deposited on different substrates. *J. Appl. Phys.* **2014**, *116*, 174307. [[CrossRef](#)]
11. Fan, Z.; Yao, K.; Wang, J. Photovoltaic effect in an indium-tin-oxide/ZnO/BiFeO₃/Pt heterostructure. *Appl. Phys. Lett.* **2014**, *105*, 162903. [[CrossRef](#)]
12. Xu, H.-M.; Wang, H.-C.; Shen, Y.; Lin, Y.-H.; Nan, C.W. Low-dimensional nanostructured photocatalysts. *J. Adv. Ceram.* **2015**, *4*, 159–182. [[CrossRef](#)]
13. Tong, H.; Ouyang, S.; Bi, Y.; Umezawa, N.; Oshikiri, M.; Ye, J. Nano-photocatalytic materials: Possibilities and challenges. *Adv. Mater.* **2012**, *24*, 229–251. [[CrossRef](#)] [[PubMed](#)]
14. Zhang, Z.; Liu, H.; Lin, Y.; Wei, Y.; Nan, C.W.; Deng, X. Influence of La doping on magnetic and optical properties of bismuth ferrite nanofibers. *J. Nanomater.* **2012**, *2012*, 1–5. [[CrossRef](#)]
15. Vanga, P.R.; Mangalaraja, R.V.; Ashok, M. Effect of co-doping on the optical, magnetic and photocatalytic properties of the Gd modified BiFeO₃. *J. Mater. Sci. Mater. Electron.* **2016**, *27*, 5699–5706. [[CrossRef](#)]
16. Singh, V.; Sharma, S.; Kumar, M.; Dwivedi, R.K. Optical Properties of Y and Ti Co-Substituted BiFeO₃ Multiferroics. In Proceedings of 58th DAE Solid State Symposium, Thapar University, Patiala, India, 17–21 December 2013.
17. Xu, X.S.; Ihlefeld, J.F.; Lee, J.H.; Ezekoye, O.K.; Vlahos, E.; Ramesh, R.; Gopalan, V.; Pan, X.Q.; Schlom, D.G.; Musfeldt, J.L. Tunable band gap in Bi(Fe_{1-x}Mn_x)O₃ films. *Appl. Phys. Lett.* **2010**, *96*, 192901. [[CrossRef](#)]
18. Liu, W.; Tan, G.; Dong, G.; Yan, X.; Ye, W.; Ren, H.; Xia, A. Structure transition and multiferroic properties of Mn-doped BiFeO₃ thin films. *J. Mater. Sci. Mater. Electron.* **2013**, *25*, 723–729. [[CrossRef](#)]
19. Huang, J.Z.; Wang, Y.; Lin, Y.; Li, M.; Nan, C.W. Effect of Mn doping on electric and magnetic properties of BiFeO₃ thin films by chemical solution deposition. *J. Appl. Phys.* **2009**, *106*, 063911. [[CrossRef](#)]

20. Feng, Y.; Wang, H.; Shen, Y.; Lin, Y.; Nan, C. Magnetic and photocatalytic behaviors of Ca Mn co-doped BiFeO₃ nanofibers. *Mod. Res. Catal.* **2013**, *2*, 1–5. [[CrossRef](#)]
21. Wang, H.C.; Lin, Y.H.; Feng, Y.N.; Shen, Y. Photocatalytic behaviors observed in Ba and Mn doped BiFeO₃ nanofibers. *J. Electroceramics* **2013**, *31*, 271–274. [[CrossRef](#)]
22. Xie, Z.; Liu, X.; Wang, W.; Wang, X.; Liu, C.; Xie, Q.; Li, Z.; Zhang, Z. Enhanced photoelectrochemical and photocatalytic performance of TiO₂ nanorod arrays/CdS quantum dots by coating TiO₂ through atomic layer deposition. *Nano Energy* **2015**, *11*, 400–408. [[CrossRef](#)]
23. Schultz, A.M.; Zhang, Y.; Salvador, P.A.; Rohrer, G.S. Effect of crystal and domain orientation on the visible-light photochemical reduction of Ag on BiFeO₃. *ACS Appl. Mater. Interfaces* **2011**, *3*, 1562–1567. [[CrossRef](#)] [[PubMed](#)]
24. Yang, S.Y.; Seidel, J.; Byrnes, S.J.; Shafer, P.; Yang, C.H.; Rossell, M.D.; Yu, P.; Chu, Y.H.; Scott, J.F.; Ager, J.W.; et al. Above-bandgap voltages from ferroelectric photovoltaic devices. *Nat. Nanotechnol.* **2010**, *5*, 143–147. [[CrossRef](#)] [[PubMed](#)]
25. Li, L.; Salvador, P.A.; Rohrer, G.S. Photocatalysts with internal electric fields. *Nanoscale* **2014**, *6*, 24–42. [[CrossRef](#)] [[PubMed](#)]
26. Chen, X.Y.; Yu, T.; Gao, F.; Zhang, H.T.; Liu, L.F.; Wang, Y.M.; Li, Z.S.; Zou, Z.G.; Liu, J.M. Application of weak ferromagnetic BiFeO₃ films as the photoelectrode material under visible-light irradiation. *Appl. Phys. Lett.* **2007**, *91*, 022114. [[CrossRef](#)]
27. Chen, X.; Liu, L.; Yu, P.Y.; Mao, S.S. Increasing solar absorption for photocatalysis with black hydrogenated titanium dioxide nanocrystals. *Science* **2011**, *331*, 746–750. [[CrossRef](#)] [[PubMed](#)]
28. Hong, S.J.; Lee, S.; Jang, J.S.; Lee, J.S. Heterojunction BiVO₄/WO₃ electrodes for enhanced photoactivity of water oxidation. *Energy Environ. Sci.* **2011**, *4*, 1781. [[CrossRef](#)]
29. Sayama, K.; Nomura, A.; Arai, T.; Sugita, T.; Abe, R.; Yanagida, M.; Oi, T.; Iwasaki, Y.; Abe, Y.; Sugihara, H. Photoelectrochemical decomposition of water into H₂ and O₂ on porous BiVO₄ thin-film electrodes under visible light and significant effect of Ag ion treatment. *J. Phys. Chem. B* **2006**, *110*, 11352–11360. [[CrossRef](#)] [[PubMed](#)]
30. Wang, L.; Fan, J.; Cao, Z.; Zheng, Y.; Yao, Z.; Shao, G.; Hu, J. Fabrication of predominantly Mn⁴⁺-doped TiO₂ nanoparticles under equilibrium conditions and their application as visible-light photocatalysts. *Chem. Asian J.* **2014**, *9*, 1904–1912. [[CrossRef](#)] [[PubMed](#)]



© 2016 by the authors; licensee MDPI, Basel, Switzerland. This article is an open access article distributed under the terms and conditions of the Creative Commons Attribution (CC-BY) license (<http://creativecommons.org/licenses/by/4.0/>).